REPORT DOCUMENTATION PAGE

Public reporting burden for this collection of information is estimated to average 1 hour per response, including the time for reviewing instructions, searching existing data sources, gathering and maintaining the data needed, and completing and reviewing this collection of information. Send comments regarding this burden estimate or any other aspect of this collection of information, including suggestions for reducing this burden to Department of Defense, Washington Headquarters Services, Directorate for Information Operations and Reports (0704-0188), 1215 Jefferson Davis Highway, Suite 1204, Arlington, VA 22202-4302. Respondents should be aware that notwithstanding any other provision of law, no person shall be subject to any penalty for failing to comply with a collection of information if it does not display a currently valid OMB control number. **PLEASE DO NOT RETURN YOUR FORM TO THE ABOVE ADDRESS.**

1. REPORT DATE *(DD-MM-YYYY)*	2. REPORT TYPE	3. DATES COVERED *(From - To)*
	Technical Papers	

4. TITLE AND SUBTITLE	5a. CONTRACT NUMBER
(Please see attached)	5b. GRANT NUMBER
	5c. PROGRAM ELEMENT NUMBER

6. AUTHOR(S)	5d. PROJECT NUMBER
	2303
	5e. TASK NUMBER
	M2C8
	5f. WORK UNIT NUMBER
	345709

7. PERFORMING ORGANIZATION NAME(S) AND ADDRESS(ES)	8. PERFORMING ORGANIZATION REPORT
Air Force Research Laboratory (AFMC) AFRL/PRS 5 Pollux Drive Edwards AFB CA 93524-7048	

9. SPONSORING / MONITORING AGENCY NAME(S) AND ADDRESS(ES)	10. SPONSOR/MONITOR'S ACRONYM(S)
Air Force Research Laboratory (AFMC) AFRL/PRS 5 Pollux Drive Edwards AFB CA 93524-7048	11. SPONSOR/MONITOR'S NUMBER(S) *Please see attached*

12. DISTRIBUTION / AVAILABILITY STATEMENT

Approved for public release; distribution unlimited.

13. SUPPLEMENTARY NOTES

14. ABSTRACT

20030129 213

15. SUBJECT TERMS

16. SECURITY CLASSIFICATION OF:			17. LIMITATION OF ABSTRACT	18. NUMBER OF PAGES	19a. NAME OF RESPONSIBLE PERSON Leilani Richardson
a. REPORT	b. ABSTRACT	c. THIS PAGE	A		19b. TELEPHONE NUMBER *(include area code)* (661) 275-5015
Unclassified	Unclassified	Unclassified			

MEMORANDUM FOR PRS (Contractor/In-House Publication)

FROM: PROI (STINFO)   24 July 2001

SUBJECT: Authorization for Release of Technical Information, Control Number: **AFRL-PR-ED-TP-2001-169**
D.T. Anderson (Univ. Wyoming); R.J. Hinde (Univ. Tennessee); S. Tam; M.E. Fajardo, "High-Resolution Spectroscopy of HCl and DCl Isolated in Solid pH_2: Direct, Induced, and Cooperative IR Transitions in a Molecular Quantum Solid"

Journal of Chemical Physics   **(Statement A)**

1. This request has been reviewed by the Foreign Disclosure Office for: a.) appropriateness of distribution statement, b.) military/national critical technology, c.) export controls or distribution restrictions, d.) appropriateness for release to a foreign nation, and e.) technical sensitivity and/or economic sensitivity.
Comments:_____
_____
_____
_____

Signature _____   Date _____

2. This request has been reviewed by the Public Affairs Office for: a.) appropriateness for public release and/or b) possible higher headquarters review.
Comments: _____
_____
_____
_____

Signature _____   Date _____

3. This request has been reviewed by the STINFO for: a.) changes if approved as amended, b) appropriateness of references, if applicable; and c.) format and completion of meeting clearance form if required
Comments:_____
_____
_____

Signature _____   Date _____

4. This request has been reviewed by PR for: a.) technical accuracy, b.) appropriateness for audience, c.) appropriateness of distribution statement, d.) technical sensitivity and economic sensitivity, e.) military/national critical technology, and f.) data rights and patentability
Comments:_____
_____

APPROVED/APPROVED AS AMENDED/DISAPPROVED

PHILIP A. KESSEL   Date
Technical Advisor
Space and Missile Propulsion Division

High-resolution spectroscopy of HCl and DCl isolated in solid parahydrogen: Direct, induced, and cooperative infrared transitions in a molecular quantum solid

David T. Anderson[a]
Department of Chemistry, University of Wyoming
Laramie, WY 82071-3838

Robert J. Hinde
Department of Chemistry, University of Tennessee
Knoxville, TN 37966-1600

Simon Tam[b] and Mario E. Fajardo
Propulsion Directorate, US Air Force Research Laboratory
AFRL/PRSP, Edwards Air Force Base, CA 93524-7680

The infrared spectroscopy and rovibrational dynamics of HCl and DCl dopants in solid parahydrogen (pH_2) were investigated using high-resolution spectroscopic methods. The absorption spectra of HCl and DCl monomers in solid pH_2 closely resemble the corresponding low temperature gas phase spectra, indicating that the gas phase vibrational and rotational quantum numbers of the impurity are conserved within the pH_2 solid. Small deviations from gas phase behavior are observed, however, such as a reduced HCl rotational energy level spacing and splitting of the fivefold orientational degeneracy of HCl rotational states with $J=2$. In addition, the pure vibrational $Q_1(0)$ ($v=1\leftarrow0$, $J=0\leftarrow0$) H_2 transition, which is infrared inactive in pure solid pH_2, is detected in the HCl doped sample. This transition is induced in pH_2 molecules by neighboring HCl molecules through a weak "overlap induction" mechanism that is the only induction mechanism operative for $J=0$ impurities in pH_2. Rovibrational transitions are also detected near the induced $Q_1(0)$ H_2 absorption; these are attributed to cooperative transitions involving single photon excitation of pH_2–HCl pairs. Detailed isotopic analysis reveals that these cooperative transitions involve pure vibrational excitation of the pH_2 and pure rotational excitation of the HCl. Two-molecule transitions have long been studied for isotopic and rotational dopants (*e.g.*, D_2, HD, orthohydrogen) in solid pH_2, but this is the first time such cooperative transitions have been attributed to a chemical impurity in pH_2 matrices.

[a]Corresponding author: danderso@uwyo.edu
[b]Present address: KLA-Tencor Corp., 1 Technology Drive, Milpitas, CA 95035

I. INTRODUCTION

The infrared (IR) absorption spectroscopy of hydrogen halide dopants HX (X = F, Cl, Br) in rare gas (Rg) solids has been studied extensively, beginning in the 1960s.[1] These studies revealed that HX dopants in rare gas solids exhibit $R(0)$, $R(1)$, and $P(1)$ rovibrational transitions, as would be expected for HX molecules at temperatures of 10 to 20 K; this indicates that the rotational motion of HX molecules embedded in rare gas matrices is only weakly hindered. For HCl dopants, this interpretation was later confirmed by observations of both the HCl $J=1\leftarrow0$ pure rotational absorption transition[2] and the rovibrational Q branch in the HCl Raman spectrum.[3] There are two main differences between the rovibrational spectrum of gas phase HCl and the spectra exhibited by HCl dopants in rare gas solids, differences which arise from the Rg–HCl intermolecular potential: a slight redshift in the vibrational band origin and a small reduction in the rotational spacing. Analysis of the spectral perturbations induced by the cryogenic matrix can therefore provide information on the rovibrational dynamics of HCl dopants in the matrix environment and the potential surface felt by these dopants in this environment.

For HCl dopants located in single substitution sites of a face centered cubic (fcc) rare gas crystal, the octahedral site symmetry effectively eliminates many of the anisotropic terms in the Rg–HCl potential; hence a dopant HCl molecule with its center of mass held fixed at the center of the substitution site feels a nearly isotropic orientational potential surface. However, if the rare gas matrix relaxes around the HCl dopant, lowering the octahedral symmetry of the substitution site, or if the HCl moves away from the center of the cavity, the potential anisotropy increases, leading to energetic barriers to the rotation of the HCl molecule in the matrix. This perturbs the rotational motion of the HCl, and can both shift the energy of excited HCl rotational states with $J>0$ and split the $(2J+1)$-fold orientational degeneracy of these states. This perturbation of the HCl rotational quantum states by angular anisotropy is historically called a crystal field effect.[4,5]

Another perturbation of the dopant rotational states results from the coupling between the dopant's translational and rotational motion.[6-8] As the HCl rotates, its minimum energy center-of-mass position in the single substitution site varies, leading to a coupling between the molecule's translational and rotational degrees of freedom as it both rotates and rattles around in

the rare gas cavity. This rotation-translation coupling can also lead to deviations of the condensed phase spectrum from the gas phase spectrum.[6-8]

With these studies in mind, we decided to investigate the infrared spectra of HCl and DCl in cryogenic solid hydrogen matrices to study the rovibrational dynamics of these species in this environment. While even neon rare gas solids are fairly well described as classical crystals, the light mass of H_2 and weakly attractive H_2–H_2 intermolecular forces conspire to make solid hydrogen a quantum solid,[9-12] with physical properties that are dominated by large amplitude zero-point motions of the individual H_2 molecules about their nominal lattice positions. In addition, because the H_2 rotational constant is large and the anisotropic components of the H_2–H_2 interaction potential are small, individual H_2 molecules retain their gas phase vibrational and rotational quantum numbers in the solid. The physical properties of these quantum solids make them ideal "solvents" in which to study the high-resolution spectroscopy and rovibrational dynamics of chemical impurities in a condensed phase. Accordingly, solid molecular hydrogen has been the subject of numerous investigations,[13-28] with both pure and doped systems receiving considerable attention.

Molecular hydrogen exists in two distinct nuclear spin modifications: orthohydrogen, in which the nuclear spins are coupled together to form a triplet spin state, and parahydrogen, in which the nuclear spins are coupled together to form a singlet spin state. Orthohydrogen (oH_2) molecules have odd rotational quantum numbers, J, while parahydrogen (pH_2) molecules have even J values. A pure orthohydrogen solid is made up of a collection of $J=1$ molecules, which, due to the threefold M_J orientational degeneracy and the permanent quadrupole moment of the $J=1$ state, can form orientationally ordered phases.[9,10] By comparison, solid parahydrogen is made up of $J=0$ molecules, which are individually spherically symmetric objects lacking any permanent electrostatic moments. Thus solid parahydrogen is a collection of spherical objects held together only by isotropic intermolecular forces, much like a rare gas solid. However, an important distinction between solid pH_2 and rare gas matrices is that the H_2 molecules that make up solid pH_2 have both rotational and vibrational degrees of freedom. In this study, we exploit this distinction to probe the microscopic dynamics of both the pH_2 host and the HCl or DCl dopant, dynamics which are mediated by the H_2–HCl intermolecular potential.

Solid pH_2 is a hexagonal close packed (hcp) crystal[10] in which nearest neighbor H_2 molecules are separated by 3.79 Å. The equilibrium distance of the pH_2–HCl intermolecular

potential surface is 3.88 Å (see below). Consequently we expect that the HCl dopant should replace a single pH$_2$ molecule in the hcp crystal. Due to the high symmetry of the single substitution site, in which the spatial distribution of the pH$_2$ molecules around the HCl is very nearly spherical, the anisotropic orientational potential felt by the HCl due to its twelve nearest neighbor pH$_2$ molecules should be exceedingly small. Hence the HCl should freely rotate with its center-of-mass located (on average) at the center of the site, as is the case when HCl is doped into rare gas solids.[1,2]

In this paper we demonstrate that HCl and DCl impurities do in fact rotate nearly freely in solid pH$_2$ matrices, so that the rotational quantum number of the impurities remains good in the matrix environment. Thus the infrared absorption transitions of HCl and DCl dopants in pH$_2$ can be labeled using gas phase notation. We adopt the standard $L_{v'}(J')$ notation for labeling (v', J') ← ($v''=0$, J'') rovibrational absorptions, in which L is given by O, P, Q, R, or S for $\Delta J = J' - J'' = -2, -1, 0, +1$, or $+2$, respectively. We find that $J=0$ HCl and DCl dopants also induce infrared activity in neighboring pH$_2$ molecules through a weak overlap induction mechanism. Finally, we report the first observations of cooperative transitions in chemically doped pH$_2$ matrices, in which a single photon excites the rotational motion of a dopant molecule and the vibrational coordinate of an adjacent pH$_2$ molecule. These two-molecule cooperative transitions are the condensed phase analogues of combination bands in van der Waals clusters.

The rest of the paper is organized as follows. In Section II we present the experimental details germane to this paper. In Section III we present, assign and partially analyze the spectroscopic data related to the direct infrared excitation of the HCl and DCl impurities. In Section IV we present and analyze our observations related to rovibrational transitions of pH$_2$ molecules in the matrix, including the pH$_2$–HCl cooperative transitions. In Section V we discuss the rovibrational dynamics of HCl dopants in a pure $v=0$ pH$_2$ solid and the rotational dynamics of HCl dopants with either a nearest neighbor $v=1$ pH$_2$ molecule or a nearest neighbor $v=1$, $J=2$ H$_2$ molecule. Finally, in Section VI we formulate our conclusions and discuss future research directions.

II. EXPERIMENT

The experimental apparatus and sample preparation techniques have been described in detail elsewhere;[26,27] here we will give only a brief summary, highlighting the specific aspects relevant to the present experiments. Doped pH$_2$ solids are prepared by rapid vapor codeposition of precooled pH$_2$ gas and room temperature HCl (or DCl) gas onto a BaF$_2$ substrate, which is cooled to $T \approx 2$ K in a liquid helium (lHe) bath cryostat. The precooled pH$_2$ is prepared in an ortho/para H$_2$ converter operated at 15 K with nH$_2$ (normal hydrogen) inlet rates ≈ 200 mmol/h, yielding a pH$_2$ flow that impinges upon the substrate at a 45° angle. The flow rate of the HCl gas is adjusted to produce samples with 10–300 parts per million (ppm) of HCl in the pH$_2$ host matrix. We prepared both samples doped with natural abundance HCl or DCl and samples doped with isotopically enriched H^{35}Cl, H^{37}Cl, D^{35}Cl, or D^{37}Cl, prepared by reaction of isotopically enriched NaCl with concentrated H$_2$SO$_4$ and D$_2$SO$_4$. The HCl and DCl doped pH$_2$ samples typically contain residual oH$_2$ (J=1) impurities at concentrations of roughly 100 ppm. However, as we describe below, some pH$_2$ samples were intentionally doped with higher concentrations of oH$_2$ by operating the ortho/para converter at elevated temperatures.

The infrared spectra of the doped pH$_2$ solids were recorded at resolutions ranging from 0.005 to 0.01 cm^{-1}; the main optical axis is parallel to the substrate normal. The Fourier transform (FT) IR spectrometer (Bruker IFS 120HR) is equipped with a glowbar source, a KBr beam splitter, and an InSb detector (1800–9000 cm^{-1}). To accommodate the IR spectroscopy, the lHe cryostat resides inside a 0.5 m^3 polycarbonate box purged with a constant flow of dry N$_2$ gas. As-deposited spectra are recorded immediately after deposition. Annealed spectra are recorded after raising the temperature of the solid to 4.8 K for a specified period of time.

In this study, we depart from our normal convention of reporting concentrations determined via the application of Beer's Law to the observed IR absorption spectra. We lack a single spectroscopic feature [e.g., the HCl or DCl monomer $R_1(0)$ line] which remains observable over the wide range of dopant concentrations employed. Instead, we report the concentration calculated as the quotient of the inlet quantities of dopant and pH$_2$. We estimate that these reported concentrations are within $\pm$ 40 % of the true dopant concentrations.

III. RESULTS AND ANALYSIS: TRANSITIONS OF HCl AND DCl DOPANTS

We begin by extracting the $J=0$ H_2 component from the full 4D H_2–HCl intermolecular potential energy surface (PES)[29] to understand the nature of the HCl substitution site in pH_2 matrices. Figure 1 shows a contour plot of the resulting pH_2–HCl intermolecular potential in a molecule fixed Cartesian coordinate system. The origin of the coordinate system is the HCl center of mass and the X-axis coincides with the HCl bond axis. The pair potential has a global minimum $V_{min}= -88.97$ cm^{-1} at $R=3.88$ Å for the linear pH_2–HCl configuration, and a local minimum $V= -65.46$ cm^{-1} at $R=3.52$ Å for the linear pH_2–ClH configuration. Because the nearest-neighbor spacing[10] in hcp crystalline pH_2 is 3.79 Å, we conclude that HCl should easily be accommodated in a single substitution site. Given the isotropic nature of a single substitution site, the modest anisotropy in the pH_2–HCl PES (see Fig. 1), and the large rotational constants[30,31] of HCl ($B=10.44$ cm^{-1}) and DCl ($B=5.39$ cm^{-1}), the total angular momentum quantum number J associated with HCl and DCl dopants in pH_2 matrices should remain a good quantum number.

A. Survey scans of HCl and DCl doped pH_2 samples

Survey scans of the HCl and DCl doped samples in the vicinity of dopant vibrational fundamental are shown in Fig. 2. As expected, the as-deposited spectrum of HCl in solid pH_2 is dominated by the $R_1(0)$ absorption feature of the H^{35}Cl and H^{37}Cl dopants present in natural abundance in the HCl sample. The isotopic label associated with each peak is easily identified from the characteristic 3:1 isotopic abundance ratio and the 2.1 cm^{-1} frequency shift[30] between the H^{35}Cl and H^{37}Cl fundamental features; these assignments are unambiguously confirmed using isotopically enriched samples (see below).

Upon annealing the sample at $T=4.8$ K for short periods of time, additional sharp features grow in irreversibly at energies below that of the HCl monomer transition. These sharp features are due to hydrogen bonded (HCl)$_n$ clusters that agglomerate in the pH_2 solid at higher temperatures following thermally-activated HCl diffusion. Furthermore, due to the characteristic shift of the HCl stretching frequency upon hydrogen bond formation, the different cluster species ($n=2, 3$, etc.) absorb at different frequencies and are well resolved in the infrared spectrum. Note that in the as-deposited sample the dominant species is the HCl monomer, attesting to the isolation efficiency of the rapid vapor deposition method.[26,27] The cluster features are of interest

due to the pervasive role that hydrogen bonding interactions play in a variety of environments,[32,33] but further discussion of these transitions is beyond the scope of the present paper and will be presented separately in a future publication.[34]

A similar spectrum is recorded for DCl doped samples in the vicinity of the DCl fundamental. Again, the spectrum of the as-deposited samples is dominated by the DCl $R_1(0)$ monomer transition, which is actually off scale in Fig. 2. The $D^{35}Cl$ and $D^{37}Cl$ isotopomers are present in the 3:1 natural isotopic abundance ratio and give rise to two features separated by the 3.0 cm^{-1} frequency difference[31] characteristic of the fundamental DCl stretch. Upon annealing the sample, sharp transitions grow in irreversibly with comparable intensity patterns and spacing to those measured in the HCl doped samples. By analogy, these additional features are ascribed to $(DCl)_n$ clusters that form in the pH_2 solid at elevated temperatures.

For both HCl and DCl dopants, some of the sharp features attributed to the clusters appear very close to the vibrational band origin of the corresponding monomer. These cluster features are presumably due to excitation of the "dangling" HCl or DCl bonds of the various cluster species. These so-called "free" or "acceptor" HCl and DCl molecules are not shifted strongly by the hydrogen bond interaction and absorb near the monomer origin.[32,33] Regardless of the specifics of the cluster assignment for these features, it is clear that they can (in principle) overlap with or obscure the monomer rovibrational transitions. However, comparison of the as-deposited and annealed samples can facilitate tentative assignments of features to isolated dopants or to clusters; these assignments can be tested via further analysis. For example, in the next section we show that a small peak at roughly 2072.2 cm^{-1} that is just discernable in the as-deposited DCl sample arises from the $P_1(1)$ transition of isolated DCl dopants.

B. DCl/pH₂ rovibrational assignment

Assignment of the DCl monomer features is done by inspection based on a model of nearly free rotation of DCl dopants in the pH_2 matrix. Based on the gas phase rotational constant[31] of DCl ($B=5.39$ cm^{-1} for $v=0$), at the highest temperature ($T=4.8$ K) accessed in these experiments, approximately 89% of the DCl molecules are in the ground $J=0$ rotational state, with 11% in $J=1$ and less than 0.03% in $J=2$. Hence the rovibrational spectrum of DCl in pH_2 should be dominated by a single $R_1(0)$ transition at low temperature with $R_1(1)$ and $P_1(1)$ transitions visible in the higher temperature scans.

Infrared spectra of isotopically enriched $D^{35}Cl/pH_2$ and $D^{37}Cl/pH_2$ samples are shown in Figs. 3 and 4, respectively. The observed transition frequencies and linewidths (full width at half maximum or FWHM) are summarized in Table I for both isotopomers. Trace (a) is the as-deposited $D^{35}Cl/pH_2$ sample in which contributions from $(D^{35}Cl)_n$ cluster absorptions are minimal. The $P_1(1)$ transition is evident in this spectrum approximately $4B$ or 20 cm^{-1} lower in energy than the strong $R_1(0)$ peak, which is off scale in the spectrum. Traces (b) through (d) show spectra recorded at T=4.8, 2.4, and 3.6 K, respectively, demonstrating the reversible temperature dependence of this monomer feature. The features near 2078 cm^{-1} assigned to $(DCl)_n$ clusters irreversibly increase in intensity during the initial annealing. The "hot" $P_1(1)$ and $R_1(1)$ rovibrational transitions at roughly 2072.2 cm^{-1} and 2102.6 cm^{-1}, respectively, can be assigned based on their reversible temperature dependence and $-4B$ and $+2B$ spacing of these features from $R_1(0)$.

The $R_1(0)$ and $P_1(1)$ transitions display no visible (≤0.1 cm^{-1}) fine structure and thus these two lines are used to calculate an effective rotational constant B_{AVG}, where $B_{AVG} = (B_{v=0} + B_{v=1})/2$. This leads to a value of $B_{AVG} = 5.1$ cm^{-1} (experimentally indistinguishable for both $D^{35}Cl$ and $D^{37}Cl$) which is close to but slightly smaller than the gas phase values[31] of 5.34 cm^{-1} for $D^{35}Cl$ and 5.32 cm^{-1} for $D^{37}Cl$. The slight reduction in B in the matrix environment arises from crystal field effects, as explained earlier. Based on this value of B_{AVG}, the DCl $R_1(1)$ transition should be observed at 2102.8 cm^{-1}. Consistent with this prediction, a "hot" rovibrational transition is detected in this region that is split into (at least) three components. The average frequency of the three resolvable features is 2102.6 cm^{-1} for $D^{35}Cl$, which is very close to the predicted $R_1(1)$ transition frequency. The origin of the splitting of the $R_1(1)$ transition will be discussed below. With this rovibrational assignment, the vibrational band origin for $D^{35}Cl$ and $D^{37}Cl$ are calculated to be $v_0 = \frac{1}{2}[R_1(0) + P_1(1)] = 2082.4$ cm^{-1} and 2079.4 cm^{-1}, respectively, each redshifted by 8.7 cm^{-1} from the corresponding gas phase value.[31]

To further verify that the $P_1(1)$ and $R_1(1)$ transitions originate from a thermally populated J=1 DCl state at approximately E_{rot}= 10.2 cm^{-1}, the temperature dependence of the integrated absorbance of these features was fit to a standard Boltzmann equation,

$$I(J' \leftarrow J'') = N_{J''}(J''+ J'+1) \exp(-2B/kT)/Q_{rot}(B, T) \qquad (1),$$

where $N_{J''}$ and B are determined via a nonlinear least squares fit to the experimental data shown in Figs. 3 and 4. $Q_{rot}(B, T)$ is the rotational partition function (calculated for a rigid rotor) and $(J''+J'+1)$ is a term that accounts for both the $(2J+1)$-fold M_J degeneracy and the Hönl-London line strength factor for the specific transition.[35] The $P_1(1)$ and $R_1(1)$ data are fit separately; the results of these fits are shown in Fig. 5. The fact that the two curves do not coincide is due to small deviations from the gas phase Hönl-London line strength factors in the matrix environment. From the two fits shown in Fig. 5 we obtain an average B value of 5 ± 1 cm^{-1}, where the quoted uncertainty represents the difference in the B values obtained from the two fits. This value is consistent with the rovibrational assignment presented above. Thus, while small deviations from gas phase behavior are observed, the appropriate first-order picture that emerges from our observations is one of nearly free rotating DCl in the pH$_2$ matrix.

One more prominent deviation from the gas phase spectrum, however, is the splitting of the $R_1(1)$ transition into three components. While the origin of this splitting cannot be unambiguously determined from the spectroscopic data alone, we speculate that it arises from a lifting of the fivefold M_J degeneracy of the $J=2$ upper rotational state that is accessed in this transition, which splits this state into three M_J components ($M_J=0, \pm1, \pm2$).[4,5] This splitting, which may signal preferential alignment of the $J=2$ rotational state with respect to the pH$_2$ crystal's c-axis, presumably arises from anisotropic terms in the orientational potential energy surface experienced by the $J=2$ DCl state in the pH$_2$ matrix. At this point further theoretical modeling is needed to interpret the observed multiplet structure, but the first-order picture remains one of nearly free rotation of the DCl dopant. Neither the $P_1(1)$ nor the $R_1(0)$ transition exhibits any visible multiplet structure. This is interpreted as evidence that, to within the linewidth of these transitions (0.2 cm^{-1} FWHM), the pH$_2$ matrix does not lift the threefold degeneracy of the $J=1$ state in either vibrational level.

C. HCl/pH$_2$ rovibrational assignment

Based on the results for DCl, our expectation is that HCl should also freely rotate in solid pH$_2$. However, due to HCl's larger rotational constant[30] ($B_{HCl}=10.44$ cm^{-1}), even at T=4.8 K the ratio of the $J=1$ to $J=0$ populations should be only 1:175 (*i.e.*, $Q_{rot} \approx 1$). Thus, the absorption spectrum of HCl in pH$_2$ should be extremely simple, consisting of a single $R_1(0)$ rovibrational

transition out of the ground $J=0$ rotational state. Based on the DCl results, this transition is expected to appear approximately 10 cm^{-1} to the red of the gas phase $R_1(0)$ transition.

In the survey scans presented in Fig. 2, a strong transition in the HCl doped sample is evident just to the red of 2900 cm^{-1}. As noted earlier, this transition displays the 3:1 isotopic abundance ratio and 2.1 cm^{-1} splitting[30] characteristic of natural isotopic abundance HCl. This feature is assigned to $R_1(0)$ based on its absolute transition frequency and relatively broad lineshape. The $R_1(0)$ transition for H^{35}Cl is at 2894.2 cm^{-1}, redshifted by 12.0 cm^{-1} from the gas phase $R_1(0)$ transition[30] at 2906.2464 cm^{-1}. If this transition were instead assigned to the $Q_1(0)$ transition, it would be blueshifted by approximately 8 cm^{-1} from the gas phase transition energy; this seems highly unlikely given the shape of the pH$_2$–HCl intermolecular PES and the "size" of a single substitution site. In addition, $Q_1(0)$ transitions of impurity species in pH$_2$ are usually very sharp because they involve pure vibrational excitation which is only weakly coupled to the pH$_2$ solid. In contrast, transitions involving $J>0$ states are generally broader, presumably due to the m re efficient coupling between the low-energy dopant rotational degrees of freedom and the phonon modes of the solid.

To verify this rovibrational assignment and to better characterize the purity of the HCl rovibrational quantum states in pH$_2$, spectra were recorded at the highest possible temperatures in order to detect transitions from thermally populated excited HCl rotational states. At $T=4.8$ K the ratio of the gas phase integrated intensities of $R_1(1)$ to $R_1(0)$ should reach 1:263, making it just possible to detect the $R_1(1)$ transition in the thickest, most concentrated samples. Indeed, a broad feature is observed for both H^{35}Cl and H^{37}Cl doped pH$_2$ solids that is approximately 2B higher in energy than the corresponding $R_1(0)$ transition. The frequencies and linewidths of these transitions are presented in Table I for both isotopomers.

An enlarged region of the monomer spectrum for the H^{35}Cl doped sample in the vicinity of the $R_1(1)$ transition is shown in Fig. 6. The different traces in this figure show the reversible temperature dependence of the feature assigned as $R_1(1)$. The $R_1(1)$ transition is most evident in trace (e), which is the spectrum recorded at $T \approx 10$ K during the destructive sublimation of the sample. Fitting the temperature dependence of the $R_1(1)$ transition intensity to Eq. (1) is not possible due to the negligibly small integrated peak intensities in most spectra. (The temperature in the subliming sample cannot be monitored with precision because the solid detaches from the substrate.) However, the temperature dependence of this peak is similar to that of the "hot" DCl

transitions, clearly indicating that this transition originates from an excited state at a significantly higher energy. Attempts to locate the corresponding HCl $P_1(1)$ transition were unsuccessful because the more concentrated sample (284 ppm H^{35}Cl) used to measure these weak "hot" rovibrational transitions exhibits significant congestion in the $P_1(1)$ region from (HCl)$_n$ cluster peaks.

The $R_1(0)$ and $R_1(1)$ transitions are both relatively broad under these conditions but permit the average rotational constant B_{AVG} of HCl in solid pH$_2$ to be estimated. For both HCl isotopomers the calculated B_{AVG} is 9.1 cm^{-1}, which is about 7% smaller than the gas phase values[30] of 9.825 cm^{-1} for H^{35}Cl and 9.811 cm^{-1} for H^{37}Cl. Assuming a $2B_{AVG}$ rotational spacing between the $R_1(0)$ transition and the vibrational origin for this band, the HCl band origin $v_0 \approx R_1(0) - 2B_{AVG} = 2876.0$ cm^{-1} is redshifted by ≈ 9.6 cm^{-1} from the gas phase value. Thus, the rovibrational spectrum of HCl in pH$_2$ closely resembles that of gas phase HCl, except that the spectrum is redshifted by roughly 10 cm^{-1} and exhibits a rotational spacing that is 93% of the gas phase value.

The spectroscopic data presented for all four HCl isotopes are therefore consistent with nearly free rotation of the HCl impurity within the pH$_2$ solid. Thus, the gas phase rotational quantum number J associated with the total angular momentum of the HCl remains an approximately good quantum number when the HCl is trapped in the pH$_2$ crystal. The nearly free rotational motion of the HCl is presumably a direct result of the large rotational constant of the hydride and the isotropic solvation site that the pH$_2$ presents to the HCl impurity.

IV. RESULTS AND ANALYSIS: pH$_2$ TRANSITIONS INDUCED BY HCl AND DCl DOPANTS

The H$_2$ $Q_1(0)$ vibrational transition is infrared inactive in pure solid pH$_2$ but is observed[13,23,36] in pH$_2$ solids doped with low concentrations of oH$_2$. The mechanism by which oH$_2$ dopants induce infrared activity associated with the $Q_1(0)$ transition of nearby pH$_2$ molecules has been studied extensively;[37] in brief, the permanent quadrupole moment of the oH$_2$ impurity generates an electrostatic field that induces transition dipoles in pH$_2$ molecules in the host matrix. This quadrupole-induced-dipole transition is inactive in pure pH$_2$ because a $J=0$ pH$_2$ molecule is a spherical object with no multipolar electrostatic field. The oH$_2$ induced $Q_1(0)$ IR absorption transition in solid pH$_2$ doped with oH$_2$ appears at 4153.1 cm^{-1} and exhibits a

characteristic lineshape with FWHM 0.4 cm^{-1} that is attributed to vibron hopping that delocalizes the $v=1$ excitation throughout the hcp pH$_2$ crystal.[37] Because this transition is only IR active if the oH$_2$ impurity undergoes a change in its M_J quantum number, it can be more fully described as a $Q_1(0) + Q_0(1)$ transition; this notation emphasizes the required presence of the oH$_2$ dopant molecule undergoing the M_J orientational transition. The oH$_2$ dopants themselves also undergo IR allowed $Q_1(1)$ transitions visible at 4146.6 cm^{-1}.

and   Strong *external* electric fields can also induce $Q_1(0)$ infrared activity in solid pH$_2$, in this case via the Condon effect.[17] However, the vibron hopping line-broadening mechanism is inactive for such a transition because the inducing field is external to the pH$_2$ crystal lattice; consequently the vibrational excitation remains localized on an individual pH$_2$ molecule and the transition is very sharp: it appears at 4149.70 cm^{-1} (with FWHM 0.03 cm^{-1}) at the low-frequency end of the vibron band. Similar narrow transitions are observed in solid pH$_2$ matrices irradiated with γ-rays;[18] these transitions are thought to arise from a Condon effect induction mechanism in which the inducing field is generated by a large number of immobile charged species distributed throughout the pH$_2$ solid. To the extent that this field is uniform over large spatial regions, it mimics the effect of an externally applied field.

We have established that HCl and DCl dopants in pH$_2$ matrices retain a good rotational quantum number J, and that the vast majority of these dopants are in the $J=0$ ground rotational state at $T=2.4$ K. Like pH$_2$ molecules, HCl and DCl molecules with $J=0$ have no permanent electrostatic field; consequently these dopants cannot induce IR activity in the pH$_2$ matrix through mechanisms based on electrostatic induction. However, $J=0$ impurities can generate IR activity in the pH$_2$ matrix via an alternative mechanism based on transition dipole moments induced by isotropic exchange and dispersion interactions, which are active even for $J=0$ species.[38,39] Consequently it may be possible to observe $Q_1(0)$ pH$_2$ transitions in our HCl and DCl doped pH$_2$ samples.

A. HCl and DCl induced $Q_1(0)$ H$_2$ transitions in solid pH$_2$ /DCl (?)

Survey scans of the H$_2$ fundamental region (4100–4200 cm^{-1}) of HCl doped pH$_2$ solids are shown in Fig. 7. Traces (a) through (d) are as-deposited samples recorded at temperatures near 2.4 K for pH$_2$ samples containing, respectively, only residual oH$_2$, HCl dopants, DCl dopants, and both HCl and DCl dopants. The very weak feature just discernable in trace (a) near

4153 cm^{-1} is the $Q_1(0)$ pH$_2$ absorption induced by residual oH$_2$ molecules in the pH$_2$ solid.[13,23] The broad absorption at the high energy end of the spectrum is the rising edge of the $Q_R(0)$ H$_2$ phonon sideband which involves vibrational excitation as well as phonon excitation.[10] The extremely sharp features near 4149.4 cm^{-1} in traces (b) through (d) are induced by the HCl and DCl dopant molecules. The frequencies and linewidths of these features are summarized in Table II. The fact that these features are observed in the vicinity of the H$_2$ vibrational fundamental, and appear at nearly the same frequency for both the HCl and DCl doped samples, supports the claim that they involve vibrational excitation localized on a pH$_2$ molecule and are not associated with vibrational or rotational excitation of the impurity; we assign these features to the $Q_1(0)$ transitions of pH$_2$ molecules adjacent to the HCl or DCl impurity. Traces (c) and (d) also show the $R_2(0)$ D^{35}Cl and D^{37}Cl overtone rovibrational transitions that serendipitously absorb in this region.

High-resolution scans of the induced $Q_1(0)$ pH$_2$ feature are shown in Fig. 8, demonstrating the extremely sharp nature of this feature in both the HCl and DCl doped solids. Traces (a) and (b) are for as-deposited D^{35}Cl and D^{37}Cl doped pH$_2$ samples, respectively, while traces (c) and (d) are for the corresponding as-deposited HCl isotopomer doped samples. The linewidths of these features are close to the experimental resolution of 0.005 cm^{-1}, allowing for very precise determinations of the transition energies. Note that given the narrowness of these features, it is easy to resolve the 0.07 cm^{-1} shift between the HCl and DCl induced features. The fact that these features depend on the mass of the dopant species is consistent with our hypothesis that these features are induced by the dopants.

The features shown in Fig. 8 appear at frequencies very close to the $Q_1(0)$ pH$_2$ transition attributed to Condon effect induction in solid pH$_2$ exposed to an external electric field; like the Condon effect transitions, these features are also very narrow. An alternative explanation for the features depicted in Fig. 8 might therefore involve Condon-type induction by the superimposed dipolar fields of the (HCl)$_2$ dimers present at low concentrations in the as-deposited samples. However, annealing of these samples does not result in the irreversible growth of these features. Instead, additional sharp lines at nearby frequencies grow in upon annealing; these lines are attributed to induction mechanisms involving HCl dimers and larger clusters. Furthermore, Fig. 9 shows that in as-deposited samples, the integrated intensity of the narrow features shown in Fig. 8 is linearly correlated with the integrated intensity of the HCl $R_1(0)$ monomer transition

over a wide range of HCl concentrations. In contrast, if these features were induced by $(HCl)_2$ dimers (or larger clusters), then the data shown in Fig. 9 would exhibit nonlinear character. Because the HCl and DCl induced features shown in Figs. 7 and 8 are present in as-deposited samples, display intensities linearly correlated with the intensities of known monomer absorptions, and do not increase in intensity upon annealing, we conclude that they are induced by HCl or DCl monomers and not by clusters. Because nearly all of the HCl and DCl monomers in our samples are in the $J=0$ rotational state, we assign these features to $Q_1(0)$ H_2 + $Q_0(0)$ HCl (or DCl) transitions; here the notation "$+Q_0(0)$" emphasizes the fact that the features are induced by $J=0$ HCl or DCl molecules.

To confirm that these features are not due to residual oH_2 molecules in the solid, samples of HCl/pH_2 were intentionally doped with higher concentrations of oH_2. The results of intentionally increasing the oH_2 concentration in pH_2 and HCl/pH_2 samples are shown in Fig. 10. Trace (a) shows the absorption spectrum at $T=2.4$ K of an as-deposited 33 ppm $H^{37}Cl$/pH_2 sample also containing roughly 100 ppm of residual oH_2. Trace (b) shows the spectrum at $T=2.5$ K of an as-deposited pH_2 sample containing 2800 ppm oH_2 and no HCl; this spectrum has been rescaled by a multiplicative factor of 0.5 for purposes of comparison. Trace (c) shows the spectrum at $T=2.4$ K of an as-deposited pH_2 sample containing both 52 ppm $H^{37}Cl$ and 1200 ppm oH_2.

The only discernable induced feature in trace (a) is the $Q_1(0)$ H_2 + $Q_0(0)$ HCl induced absorption; no oH_2 induced H_2 transitions are visible in this spectrum. In trace (b), the $Q_1(1)$ oH_2 pure vibrational transition is evident at 4146.65 cm^{-1} and the oH_2 induced $Q_1(0)$ pH_2 transition is observed at 4153.1 cm^{-1}. The frequencies and linewidths of these induced H_2 transitions agree with literature values.[13,23] Enrichment with oH_2 [trace (c)] does not increase the intensity of the HCl induced feature at 4149.4 cm-1, thereby ruling out the possibility that this feature is oH_2 dependent. New absorption features near 4139.65, 4143.11, and 4149.66 cm^{-1}, marked with asterisks, appear only in the oH_2 enriched HCl doped sample; assignment of these features, which are presumably due to oH_2-HCl clusters, is beyond the scope of the present paper.

It should be emphasized that the $J=0$ HCl induced $Q_1(0)$ H_2 transition is extremely weak. The main reason that it is detected in the current experiment is that the transition is very sharp, which permits it to be detected using high-resolution FTIR methods. In fact, if the DCl-induced transitions were only a factor of two broader (and with the same integrated intensity) they would

probably have remained undetected at the current signal-to-noise levels. The very narrow linewidth of the $Q_1(0)$ transition is intriguing; as we discuss in more detail later, it suggests that the pH$_2$ molecule(s) involved in this transition are decoupled from the rest of the pH$_2$ solid.

At present it is not known why, as Fig. 8 shows, the HCl induced $Q_1(0)$ feature is considerably more intense than the DCl induced feature (even after accounting for differences in concentration and spectral resolution). The origin of the small satellite peak to the blue of the $Q_1(0)$ transition in the HCl doped samples is also not clear at this time.

B. Cooperative pH$_2$-HCl transitions in solid pH$_2$

In both the HCl and DCl doped samples, fairly broad features are observed in Fig. 7 at energies slightly above that of the $Q_1(0)$ H$_2$ transition. The frequencies of these dopant induced absorption features depend on the rotational constant of the impurity. For example, in HCl doped pH$_2$, the first broad doublet feature is approximately 20 cm^{-1} above the pH$_2$ $Q_1(0)$ transition, while in the DCl doped sample the analogous feature is only 10 cm^{-1} above the pH$_2$ $Q_1(0)$ transition. This suggests that the spacings between these broad features and the induced $Q_1(0)$ H$_2$ peak are not accidental, but rather are determined by the $J=0 \rightarrow 1$ rotational spacing of the HCl or DCl impurity. Furthermore, the integrated intensities of these transitions correlate linearly with the intensity of the $R_1(0)$ monomer transitions (see Fig. 9). Accordingly, these transitions are assigned to $Q_1(0)$ pH$_2$ + $R_0(0)$ HCl (or DCl) cooperative transitions in which the dopant molecule undergoes a pure rotational transition in concert with the pure vibrational transition of the pH$_2$ molecule. In these transitions, a single infrared photon excites both the *rotational* coordinate of the HCl or DCl impurity and the *vibrational* coordinate of a nearby pH$_2$ molecule. In the language of van der Waals cluster spectroscopy, these transitions correspond to combination bands.

The detailed rovibrational assignments presented in Fig. 7 are conducted by correlating the gas phase rotational spacing of the dopant with the frequency difference between the cooperative transition and the impurity induced $Q_1(0)$ peak. For example, the peak labeled $Q_1(0)$ H$_2$ + $R_0(0)$ HCl in trace (b) of Fig. 7 is approximately $2B_{HCl}$ or 20 cm^{-1} higher in energy than the HCl induced $Q_1(0)$ H$_2$ transition. Similarly, the first peak to the blue of the DCl induced $Q_1(0)$ H$_2$ transition is approximately $2B_{DCl}$ or 10 cm^{-1} higher in energy than the $Q_1(0)$ transition. Absorption features blue shifted by roughly $6B$ from the $Q_1(0)$ transition are also observed in

both the HCl and DCl doped pH$_2$ samples. Based on this approximate $6B$ spacing for both isotopomers, these features are assigned to $Q_1(0)$ H$_2$ + $S_0(0)$ HCl (DCl) cooperative transitions.

In the DCl doped samples the $Q_1(0)$ H$_2$ + $S_0(0)$ DCl transition is observed near 4180 cm^{-1} with a partially resolved multiplet structure that is presumably due to anisotropic interactions that lift the M_J degeneracy of the DCl J=2 state. In the case of HCl, the $Q_1(0)$ H$_2$ + $S_0(0)$ HCl transition appears in the low-energy portion of the $Q_R(0)$ phonon sideband. Thus, in order to examine the lineshape of this cooperative transition, we recorded the absorption spectra of two samples with the same amount of pH$_2$ but with different HCl concentrations and subtracted one spectrum from the other. Because the only difference between the two samples is the concentration of HCl, the $Q_R(0)$ phonon band is removed by subtraction leaving only the HCl induced features, as shown in Fig. 11. This figure clearly shows the $Q_1(0)$ H$_2$ + $S_0(0)$ H^{35}Cl peak at roughly 4209 cm^{-1}. Note that this transition is somewhat broader than the corresponding $Q_1(0)$ H$_2$ + $S_0(0)$ DCl feature shown in Fig. 7, and lacks any discernable fine structure. This is presumably due to the better resonance matching of the HCl rotation with the pH$_2$ phonon density of states, which allows for faster relaxation of the HCl rotation.

The $Q_1(0)$ H$_2$ + $R_0(0)$ HCl (DCl) transitions are shown on an expanded scale in Fig. 12. The difference between the $Q_1(0)$ peak and the average of the frequencies of the $Q_1(0)$ H$_2$ + $R_0(0)$ HCl doublet feature (weighted by the approximate 2:1 intensity ratio) is the J=0→1 rotational spacing of a v=0 state HCl molecule next to a v=1 pH$_2$ molecule. This gives B=10.22 cm^{-1} and 10.20 cm^{-1} for the H^{35}Cl and H^{37}Cl isotopes, respectively, values which are very close to the H^{35}Cl gas phase value[30] of 10.44 cm^{-1}. A similar analysis gives B=5.22 and 5.20 cm^{-1} for D^{35}Cl and D^{37}Cl, respectively, as compared with the corresponding D^{35}Cl gas phase value[29] of B=5.392 cm^{-1}. These B values compare favorably with the B_{AVG} values determined from the direct infrared spectroscopy and with the less precise value of B determined in the Boltzmann analysis. However, the three B values measure slightly different quantities; B_{AVG} is averaged over HCl vibrational state; the B value determined in the thermal analysis is for HCl (v=0) surrounded by ground vibrational state pH$_2$, and the B value determined from analysis the cooperative transitions is for HCl (v=0) next to a vibrationally excited pH$_2$ molecule. Thus, subtle differences in the the three B values are not unexpected.

The spectra shown in Fig. 12 are for the isotopically enriched samples, so the multiplet structure observed in the $Q_1(0)$ H$_2$ + $R_0(0)$ HCl (DCl) transition is not due to different

isotopomers. The splitting is in fact a direct measurement of the splitting of the threefold degeneracy of the $J=1$ rotational state of the HCl (DCl) monomer by an adjacent vibrationally excited pH$_2$ molecule. This splitting is 1.130 cm^{-1} and 1.156 cm^{-1} for HCl and DCl, respectively. No splitting of the $J=1$ rotational state was measured for HCl surrounded by ground vibrational state pH$_2$ molecules. This implies that excitation of a neighboring pH$_2$ molecule changes qualitatively the orientational PES of the HCl (DCl) impurity in the matrix environment. The isotopic dependence of the observed splitting is consistent with this interpretation. The absolute magnitude of the splitting is approximately the same for HCl and DCl, which means that relative to the $J=1$ to $J=0$ free rotational spacing, the splitting is a factor of two larger for DCl. A larger relative splitting for DCl is expected because the smaller rotational constant of DCl makes it easier to perturb the dopant's rotational motion by anisotropic terms in the PES. We will return to this point below.

Another striking observation is the difference in the linewidths for the $Q_1(0)$ pH$_2$ pure vibrational excitation and the cooperative transitions $Q_1(0)$ H$_2$ + $R_0(0)$ HCl or $Q_1(0)$ H$_2$ + $S_0(0)$ HCl. The linewidth of the $Q_1(0)$ + $R_0(0)$ cooperative transitions are in almost quantitative agreement with the linewidths measured for the corresponding $R_1(0)$ transitions of the HCl and DCl monomers. This again is interpreted as evidence that these transitions involve excited rotational states whose rotational degrees of freedom couple more strongly with the phonon modes of the solid than does a pure vibrational transition The fact that the $Q_1(0)$ H$_2$ + $S_0(0)$ HCl linewidths are broader than those for DCl is because the cooperative transitions involving HCl dopants are more nearly resonant with the peak of the pH$_2$ phonon modes, resulting in faster dephasing and relaxation of HCl ($J=2$) compared to DCl ($J=2$).

Finally, we comment briefly on the relative integrated intensities of the induced $Q_1(0)$ H$_2$ transitions and the cooperative $Q_1(0)$ + $R_0(0)$ and $Q_1(0)$ + $S_0(0)$ transitions. As Figs. 7 and 11 show, the integrated intensities of the cooperative transitions are much larger than that of the pure vibrational $Q_1(0)$ H$_2$ transition. This is because two different induction mechanisms give rise to these spectral features. As we have explained, the IR activity of the pure vibrational $Q_1(0)$ H$_2$ transition arises from transition moments induced by isotropic overlap and dispersion interactions; these transition moments are fairly weak.[38] In the cooperative transitions, however, the upper state involves a $J>0$ HCl (DCl) impurity which is no longer isotropic and therefore exhibits a multipolar electrostatic field. This field induces a vibrational transition dipole in the

neighboring pH_2 molecule undergoing the $Q_1(0)$ transition, so that the cooperative transitions are much stronger than the pure vibrational transition.

C. HCl perturbed $S_1(0)$ H_2 transitions

Another induced zero phonon pH_2 transition that is observed in these studies is the $S_1(0)$ H_2 transition near 4486.1 cm^{-1}, which corresponds to rovibrational excitation of a single pH_2 molecule ($v=1\leftarrow0$, $J=2\leftarrow0$). In pure pH_2 solids the $S_1(0)$ H_2 transition is IR active because the hcp crystal lattice lacks inversion symmetry.[10] Spectra in the vicinity of the $S_1(0)$ transition are shown in Fig. 13 for both HCl and DCl doped pH_2 samples. The pure pH_2 transition at 4486.1 cm^{-1} is nearly optically black for these 3-mm-thick pH_2 samples, but weak transitions are observed slightly to the red of this feature in both the HCl and DCl doped samples. The positions of these features do not change to within experimental uncertainty for the individual ^{35}Cl and ^{37}Cl isotopomers. The intensity of this additional feature scales linearly with HCl dopant concentration. Thus, the new transition is assigned to the $S_1(0)$ transition of pH_2 with a neighboring HCl or DCl molecule.

The HCl perturbed $S_1(0)$ transition is shifted 5.4 cm^{-1} to the red of the pure pH_2 $S_1(0)$ transition; this shift arises from intermolecular interactions between the HCl dopant and the $v=1$, $J=2$ state of H_2. Interestingly, the corresponding redshift for the DCl perturbed feature is significantly larger at 7.0 cm^{-1}. Such a large isotope effect (1.6 cm^{-1}) for a transition that is localized on a neighboring pH_2 molecule is unusual. In the case of the induced $Q_1(0)$ H_2 transition, by comparison, the spacing between the features induced by HCl and DCl impurities was only 0.07 cm^{-1}. The large isotopic dependence of the perturbed $S_1(0)$ pH_2 transition suggests that the $J=0$ HCl and DCl molecules interact differently with the vibrationally excited $J=2$ pH_2 molecule. Furthermore, attempts to identify cooperative transitions built off the $S_1(0)$ transition that involved HCl or DCl free rotational excitation were unsuccessful. These findings are consistent with a model in which the $J=2$ excited rotational state of the pH_2 molecule strongly hinders the rotational motion of the neighboring HCl or DCl species. If this is the case, one would expect that the DCl rotational motion would be more strongly perturbed than the HCl rotational motion due to the smaller free rotor spacing for the DCl species. Consequently the shift of the HCl or DCl perturbed $S_1(0)$ transition from the pure pH_2 $S_1(0)$ transition reflects changes in the rotational or librational zero point energy of the HCl or DCl impurity. Attempts

to confirm this interpretation by modeling the rotational motion of the nominal $J=2$ H$_2$ + $J=0$ HCl (DCl) pair are currently underway.

IV. DISCUSSION

A. HCl and DCl dynamics in solid pH$_2$

The direct infrared excitation spectra of HCl and DCl provide quantitative measurements of how the vibration and rotational dynamics of these species change when solvated in solid pH$_2$. For HCl and DCl, solvation in solid pH$_2$ redshifts the vibrational frequencies by 8.7 and 9.6 cm^{-1}, respectively, from the corresponding gas phase values. This indicates that the $v=1$ impurity is lowered in energy upon solvation to a greater extent than the $v=0$ impurity. Such an interpretation agrees with the IR spectroscopy of pH$_2$-HCl van der Waals cluster, which measured a -1.09 cm^{-1} shift in the HCl fundamental vibration upon complexation.[29] The redshifts observed here therefore provide further experimental information on the dependence of the pH$_2$–HCl potential on the HCl stretching coordinate.

The spectra also provide information on the dependence of the pH$_2$–HCl potential on the rotational degrees of freedom of the HCl monomer. It is clear from the spectroscopic analysis presented above that the total angular momentum quantum number of the HCl and DCl impurities remains reasonably good in the pH$_2$ solid. However, the $J=0\rightarrow1$ rotational energy spacing of HCl or DCl dopants in pH$_2$ is 4-7 % less than that of isolated HCl or DCl molecules in the gas phase. This suggests that upon solvation in pH$_2$, the $J=1$ state of both impurities is lowered in energy by a greater amount than the $J=0$ state, perhaps because the $J=1$ state can preferentially sample attractive portions of the pH$_2$–HCl PES shown in Fig. 1.

The $R_1(1)$ transition of the DCl isotopomer in pH$_2$ exhibits both a reduced rotational spacing and visible multiplet structure. The observed splitting is interpreted as evidence that the $J=2$ rotational state accessed in this transition can interact with the pH$_2$ matrix through higher order anisotropic terms in the intermolecular potential. Thus, while the $J=1$ state is lowered in energy but not split into resolvable sublevels, the $J=2$ state is both lowered and split into sublevels. This is in accord with elegant symmetry arguments that indicate in a perfect D_{3h} hcp crystal site the magnitude of the splitting of a $J=2$ rotational state is significantly greater than that of a $J=1$ rotational state.[4,5] While such arguments do not take into account any distortion of the pH$_2$ crystal structure around the impurity, they provide a valid first-order description of our

observations. All of these findings point to a recurring theme throughout this study, which is that the dynamics of the solute and solvent are intimately coupled.

B. Dynamics of pH_2-HCl pairs in solid pH_2

The cooperative transitions built off of the impurity induced $Q_1(0)$ H_2 pure vibrational transition provide a quantitative energy level diagram for the rotational states of HCl next to a single vibrationally excited pH_2 molecule in solid pH_2. Figure 14 compares the gas phase HCl and DCl rotational energy levels with the rotational energies determined spectroscopically from the cooperative transitions. For the low rotational states ($J=1$ and $J=2$) of HCl and DCl, the rotational level spacing in pH_2 is almost identical to the gas phase. This again validates the assertion that the HCl and DCl species retain their gas phase quantum number J in the pH_2 solid. Yet there is also a clear splitting in the rotational levels in the condensed phase that are absent in the gas phase, which is thought to be due to a lifting of the M_J degeneracy of the excited rotational states by the presence of a neighboring $v=1$, $J=0$ pH_2 molecule. The vibrational excitation of the nearest neighbor pH_2 molecule breaks the symmetry of the single substitution site and defines the pair axis between the vibrationally excited pH_2 and HCl as the new symmetry axis. We can develop a qualitative picture of the HCl rotational dynamics under the assumption that this axis is the M_J quantization axis; we will use the label k to represent the projection of the $J=1$ rotor angular momentum onto this axis in order to emphasize the analogy between the rotational dynamics of the pH_2–HCl pair in solid pH_2 and the rotational dynamics of the gas phase pH_2–HCl van der Waals dimer.[29]

In the case of the $J=1$ state, the approximate 1.3 cm^{-1} splitting and the nearly 1:2 intensity ratio between the two transitions suggests that the lower energy transition (weaker) accesses the $k=0$ state while the higher energy feature (stronger) accesses the $k=\pm 1$ state. The same energetic ordering of k states has been calculated for internal rotor states of the gas phase pH_2-HCl dimer that correlate with $J=1$ HCl.[40] In the gas phase dimer, the $J_{HCl}=1$, $k=0$ state is lower in energy because the wavefunction for this state preferentially samples the global minimum of the pH_2–HCl PES in which the HCl points toward the H_2 (i.e., the global minimum shown in Fig. 1). In contrast, the $J_{HCl}=1$, $k=\pm 1$ internal rotor state wavefunction has a maximum probability density that corresponds to the HCl bond being at nearly right angles with respect to the pair axis,

corresponding to the saddle point between the two minima in Fig. 1; thus the $J_{HCl}=1$, $k=\pm 1$ internal rotor state has a higher energy.

If this model is correct, the $J=2$ HCl and DCl states accessed in the $Q_1(0) + S_0(0)$ cooperative transitions should also be split into triplets with $k=0$, ± 1, and ± 2. However, the splitting of the $J=2$ state is not resolved as cleanly as that for the $J=1$ state due to broadening of the transition and dilution of the oscillator strength over a greater number of sublevels. The $Q_1(0) + S_0(0)$ transition may also be weaker since it derives the bulk of its intensity from the quadrupole moment of HCl while the $Q_1(0) + R_0(0)$ transition depends largely on the dipole moment of HCl. Nonetheless, the $Q_1(0) + S_0(0)$ shown in trace (c) of Fig. 7 exhibits two main peaks that are separated by 1.49 cm^{-1}, possibly with some weaker features at higher energy. In the case of HCl (Fig. 11) the corresponding transition is rather broad (8 cm^{-1} FWHM), which may in part be due to crystal field effects.

In addition, since the impurities are confined to single substitution sites, there may be a strong couplings between translational and rotational degrees of freedom. The resultant splitting of the HCl M_J rotational sublevels accessed in the cooperative transitions will therefore be affected by rotation-translation coupling between these two low energy motions. Based upon simple particle-in-a-box ideas, the "excited" translational states should be at energies comparable to the HCl and DCl rotational energy spacings, possibly leading to strongly coupled motions.

Due to the extensive zero-point motion of the pH$_2$ solid, a rigorous analysis of the coupling between the three translational and two rotational coordinates of the HCl dopant must also account for translational motion of the pH$_2$ molecules and the possible correlations between these motions. Such a rigorous treatment is possible using quantum Monte Carlo (QMC) techniques, provided an accurate intermolecular PES is available. The data presented here describing HCl rotational motion in the pH$_2$ matrix provide the experimental observables that could be used to test rigorous QMC calculations using a trial pH$_2$–HCl PES that includes dependence on the intramolecular stretching coordinates. Such a theoretical treatment of the HCl rotational motion in a single substitution site, when combined with the high-resolution data presented here, should provide a full microscopic picture of the quantum dynamics of the HCl impurities in solid pH$_2$.

Another important finding of the present study is that the goodness of the HCl J quantum number is dependent on the $J=0$ nature of the pH$_2$ solvent. The anomalous isotopic dependence

of the HCl perturbed H_2 $S_1(0)$ transition (Fig. 13), and our failure to observe cooperative transitions built off of this feature, are taken as evidence that the $J=2$ H_2 molecule restricts the rotational motion of the HCl impurity, transforming it from one of free rotation to libration.

C. $J=0$ HCl induced $Q_1(0)$ H_2 transition

The sharp features shown in Fig. 8 are assigned to pure vibrational $Q_1(0)$ excitation of pH_2 molecules. Although the $Q_1(0)$ transition is IR inactive in pure pH_2, it becomes active in the doped pH_2 solids studied here through the induction of transition dipole moments via an isotropic overlap mechanism which is the only induction mechanism operative for spherical impurities. The magnitudes of these transition moments are expected to be particularly sensitive to the pH_2–HCl distance;[38] consequently the features shown in Fig. 8 represent a rich source of information about the microscopic structure of the HCl and DCl substitution sites in pH_2 solids. An earlier report[26] shows that spherical atomic impurities such as Xe also induce IR absorption near 4150 cm^{-1}, presumably arising from a similar mechanism. It is interesting to note that analogous features induced by $J=0$ D_2 or HD impurities in solid pH_2 have never been reported, despite numerous comprehensive high-resolution studies of isotopically substituted solid hydrogens.[13,23] This may be because these transitions are obscured by the broad $Q_1(0)$ feature induced by residual oH_2 molecules typically present in these samples.

The sharpness and absolute frequency of the $Q_1(0)$ transition induced by HCl or DCl may at first seem surprising because the $Q_1(0)$ transition induced by oH_2 is much broader (0.4 cm^{-1} FWHM) and occurs at a significantly higher frequency (4153.10 cm^{-1}).[16,23] In contrast, the linewidth of the HCl induced $Q_1(0)$ feature is 0.01 cm^{-1} and substantially redshifted to 4149.39 cm^{-1}. The linewidth and redshift of this transition are intimately linked because as the vibrational frequency of the pH_2 molecule next to the impurity becomes detuned from the vibrational frequency of the other pH_2 molecules in the matrix, the probability for vibron hopping to neighboring molecules drops dramatically. Thus, once the $Q_1(0)$ pH_2 vibration is excited it remains strongly localized next to the $J=0$ HCl impurity molecule, which constitutes a "vibron sink" in the matrix.

V. CONCLUSIONS

We present here high-resolution IR studies of solid pH_2 doped with HCl and DCl impurities. By utilizing the rapid vapor deposition method developed by Fajardo and coworkers,[26,27] we show that it is possible to synthesize millimeter thick, optically transparent samples of HCl doped pH_2 solids that are amenable to high-resolution spectroscopic investigation. This approach is shown to produce well-isolated HCl species at dopant concentrations of 10 to 100 ppm. Warming the sample to temperatures above 4 K permits diffusion of the HCl species through the pH_2 solid resulting in the formation of $(HCl)_n$ clusters. The current study focuses on the rotational and vibrational dynamics of isolated HCl species in the pH_2 solid.

This study indicates, as expected, that HCl and DCl undergo nearly free internal rotation inside the pH_2 solid. This is taken as evidence that the HCl occupies a single substitution site in the hcp crystalline structure, because such a site is a nearly isotropic cavity in which the HCl molecule can freely rotate. For both HCl and DCl, the nearly free rotational dynamics are inferred from the close resemblance between the condensed phase spectrum and the hypothetical low temperature gas phase spectrum.

In addition, a weak, extremely narrow, weak absorption feature is observed near 4149.4 cm^{-1} which is assigned to a pure vibrational $Q_1(0)$ pH_2 transition induced by $J=0$ HCl and DCl impurites through an isotropic overlap induction mechanism. Thus, the observed frequency and intensity of this feature is sensitively related to the pH_2–HCl interaction potential and to the properties of the HCl doped quantum solid. Interestingly, similar induced transitions have been observed[26] for pH_2 samples doped with atoms such as Xe, but never before been reported for pH_2 solids containing $J=0$ molecular impurities.

The present assignment of the pH_2 $Q_1(0)$ transition is confirmed by (i) investigation of oH_2 enriched samples that show that the intensity of this feature is independent of the oH_2 concentration and (ii) the observation of cooperative transitions built off of the pH_2 $Q_1(0)$. These cooperative transitions involve pure vibrational excitation of the pH_2 molecule in concert with pure rotational excitation of the HCl (or DCl) impurity, and exhibit the expected dependence on the rotational constant of the impurity. These cooperative transitions are apparently a general phenomenon associated with small molecular dopants embedded in pH_2 matrices, as we have observed them for pH_2 solids doped with a wide variety of impurities.[41] Because the rapid vapor

deposition method used here makes it possible to incorporate nearly any type of chemical impurity into solid pH_2, these cooperative transitions offer new insight into the dynamics of molecules solvated in a quantum solid.

VI. ACKNOWLEDGEMENTS

REFERENCES

1. H. E. Hallam, *Vibrational Spectroscopy of Trapped Species* (Wiley, New York, 1973).
2. W. G. Von Holle and D. W. Robinson, *J. Chem. Phys.* **44**, 53, 3768 (1970).
3. L. C. Brunel, J. C. Bureau, and M. Peyron, *Chem. Phys.* **28**, 387 (1978).
4. L. Pauling, *Phys. Rev.* **36**, 430 (1930).
5. A. F. Devonshire, Proc. Roy. Soc. A **153**, 601 (1936).
6. H. Friedmann and S. Kimel, *J. Chem. Phys.* **43**, 3925 (1965).
7. H. Friedmann and S. Kimel, *J. Chem. Phys.* **44**, 4359 (1966).
8. H. Friedmann and S. Kimel, *J. Chem. Phys.* **47**, 3589 (1967).
9. I. F. Silvera, *Rev. Mod. Phys.* **52**, 393 (1980).
10. J. Van Kranendonk, *Solid hydrogen: theory of the properties of solid H_2, HD, and D_2* (Plenum Press, New York, 1983).
11. T. Oka, *Annu. Rev. Phys. Chem.* **44**, 299 (1993).
12. T. Momose and T. Shida, *Bull. Chem. Soc. Jpn.* **71**, 1 (1998).
13. M.-C. Chan, M. Okamura, C. M. Gabys, L.-W. Xu, B. D. Rehfuss, and T. Oka, *Phys. Rev. Lett.* **66**, 2060 (1991).
14. M.-C. Chan, L.-W. Xu, C. M. Gabrys, and T. Oka, *J. Chem. Phys.* **95**, 9404 (1991).
15. T. Momose, D. P. Weliky, and T. Oka, *J. Mol. Spectrosc.* **153**, 760 (1992).
16. T. Momose, K. E. Kerr, D. P. Weliky, C. M. Gabrys, R. M. Dickson, and T. Oka, *J. Chem. Phys.* **100**, 7840 (1994).
17. K. E. Kerr, T. Momose, D. P. Weliky, C. M. Gabrys, and T. Oka, *Phys. Rev. Lett.* **72**, 3957 (1994).

18. D. P. Weliky, K. E. Kerr, T. J. Byers, Y. Zhang, T. Momose, and T. Oka, *J. Chem. Phys.* **105**, 4461 (1996).

19. T. Momose, *J. Chem. Phys.* **107**, 7695 (1997).

20. T. Momose, M. Miki, T. Wakabayashi, T. Shida, M.-C. Chan, S. S. Lee, and T. Oka, *J. Chem. Phys.* **107**, 7707 (1997).

21. T. Momose, H. Katsuki, H. Hoshina, N. Sogoshi, T. Wakabayashi, and T. Shida, *J. Chem. Phys.* **107**, 7717 (1997).

22. H. Hoshina, T. Wakabayashi, T. Momose, and T. Shida, *J. Chem. Phys.* **110**, 5728 (1999).

23. R. A. Steinhoff, K. V. S. R. Apparao, D. W. Ferguson, K. N. Rao, B. P. Winnewisser, and M. Winnewisser, *Can. J. Phys.* **72**, 1122 (1994).

24. M. Mengel, B. P. Winnewisser, M. Winnewisser, *Phys. Rev. B* **55**, 10420 (1997).

25. M. Mengel, B. P. Winnewisser, M. Winnewisser, *J. Mol. Spectrsc.* **188**, 221 (1998).

26. S. Tam and M. E. Fajardo, *J. Chem. Phys.* **108**, 4237 (1998).

27. S. Tam and M. E. Fajardo, *Rev. Sci. Instr.* **70**, 1926 (1999).

28. S. Tam and M. E. Fajardo, H. Katsuki, H. Hoshina, T. Wakabayashi, and T. Momose, *J. Chem. Phys.* **111**, 4191 (1999).

29. D. T. Anderson, M. D. Schuder, and D. J. Nesbitt, *Chem. Phys.* **239**, 253 (1998).

30. C. P. Rinsland, M. A. H. Smith, A. Goldman, V. M. Devi, and D. C. Benner, *J. Mol. Spectrosc.* **159**, 274 (1993).

31. M. D. Schuder, D. D. Nelson, Jr., and D. J. Nesbitt, *J. Chem. Phys.* **94**, 5796 (1991).

32. M. D. Schuder, C. M. Lovejoy, R. Lascola, D. J. Nesbitt, *J. Chem. Phys.* **99**, 4346 (1993).

33. M. D. Schuder, D. D. Nelson, Jr., and D.J. Nesbitt, *J. Chem. Phys.* **99**, 5445 (1993).

34. D. T. Anderson, S. Tam, and M. E. Fajardo (in preparation).

35. G. Herzberg, *Infrared and Raman Spectra* (Van Nostrand-Reinhold, New York, 1945).

36. H.P. Gush, W.F.J. Hare, E.J. Allin, and H.L. Welsh, *Can. J. Phys.* **38**, 176 (1960).

37. J. van Kranendonk, *Can. J. Phys.* **38**, 240 (1960).

38. R. J. Hinde, *Phys Rev. B* **61**, 11451 (2000).

39. R. J. Hinde (in preparation).

40. D. T. Anderson and D. J. Nesbitt (unpublished results).

41. R. J. Hinde, D. T. Anderson, S. Tam, and M. E. Fajardo (in preparation).

Table I. Transition frequencies for HCl and DCl rovibrational transitions observed in solid pH_2 at T $\approx$ 2.4 K. Linewidths (FWHM) are given in parentheses. All values are in units of cm^{-1}.

transition	$H^{35}Cl$	$H^{37}Cl$	$D^{35}Cl$	$D^{37}Cl$
$P_1(1)$	---[a]	---[a]	2072.183 (0.17)	2069.273 (0.20)
$R_1(0)$	2894.19 (1.2)	2892.06 (1.1)	2092.57 (0.16)	2089.52 (0.17)
$R_1(1)$ {	2912.4 (3.3)	2910.3 (4.8)	2101.31 (0.5)	2098.29 (----)[b]
			2102.59 (0.6)	2099.60 (0.3)
			2103.89 (0.4)	2100.98 (0.4)
$R_2(0)$	5663.9 (2)	5659.9 (2)	4121.05 (0.2)	4115.17 (0.3)

[a] obscured by cluster absorptions
[b] overlapping structure

Table II. Transition frequencies for HCl and DCl induced H_2 rovibrational transitions observed in as-deposited solid pH_2 samples at T $\approx$ 2.4 K. Linewidths (FWHM) are given in parentheses. All values are in units of cm^{-1}.

Transition	$H^{35}Cl$	$H^{37}Cl$	$D^{35}Cl$	$D^{37}Cl$
$Q_1(0)$	4149.394 (0.011)	4149.391 (0.012)	4149.318 (0.02)	4149.314 (0.02)
$Q_1(0) + R_0(0)$ {	4169.02 (0.21)	4169.05 (---)[a]	4158.99 (0.09)	4158.92 (0.15)
	4170.18 (0.70)	4170.16 (0.9)	4160.16 (0.18)	4160.10 (0.23)
$Q_1(0) + S_0(0)$ {	4209 (8)	(---)[b]	4179.77 (---)[a]	4179.71 (---)[a]
			4181.26 (---)[a]	4181.28 (---)[a]
$S_1(0)$	4480.73 (0.27)	4480.73 (0.27)	4479.14 (0.23)	4479.13 (0.2)

[a] overlapping structure
[b] not determined
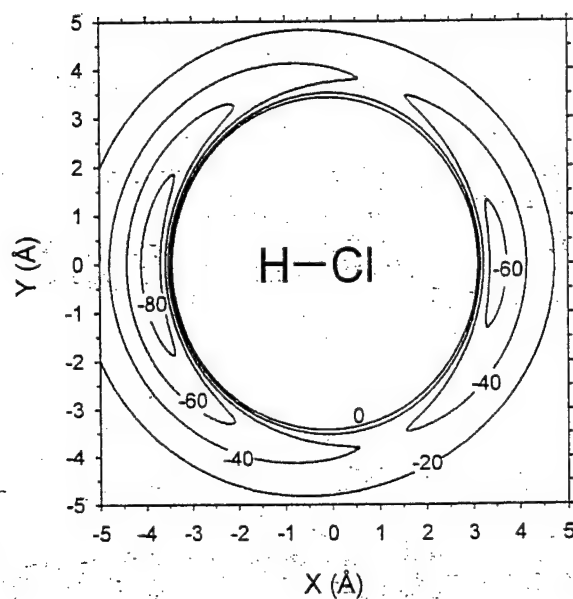
FIG. 1. Contour plot of the attractive region of the H_2-HCl *ab initio* intermolecular potential with contours spaced at 20 cm^{-1} intervals. The angular orientation of the H_2 is assumed to be isotropic, reducing the full 4D intermolecular potential to an effective 2D surface. The H_2 and HCl bond lengths are held fixed. Note the nearly circular zero contour.
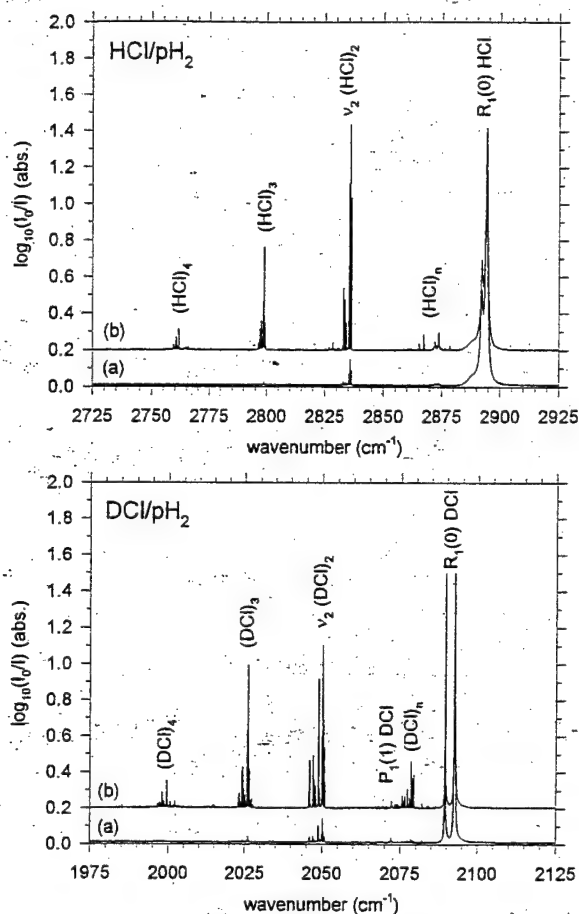
FIG. 2. HCl/pH$_2$ and DCl/pH$_2$ survey IR absorption spectra with Cl present at natural isotopic abundance. The upper panel shows spectra (0.0075 cm^{-1} resolution) of a 2.9-mm-thick 88 ppm HCl/pH$_2$ solid at $T = 2.4$ K; trace (a) is for the as-deposited sample, while trace (b) is for the same sample recooled to $T = 2.4$ K after annealing at $T = 4.8$ K for 1 hour. The lower panel shows spectra (0.01 cm^{-1} resolution) of a 3.0-mm-thick 102 ppm DCl/pH$_2$ solid at $T = 2.5$ K; trace (a) is as-deposited, while trace (b) is taken at $T = 2.4$ K after annealing at $T = 4.9$ K for 1 hour. In both samples the annealing process results in irreversible growth of the cluster absorptions.
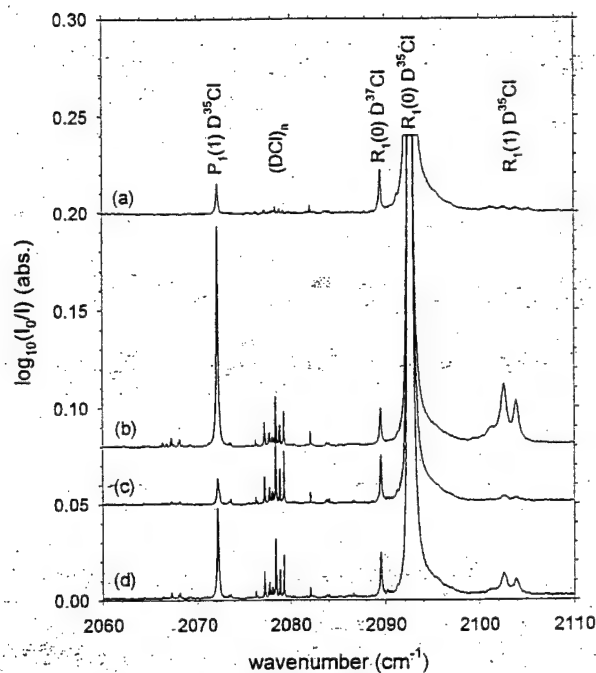
FIG. 3. Temperature dependence of $D^{35}Cl/pH_2$ monomer fundamental absorptions (0.1 cm^{-1} resolution). The sample is a 3.1-mm-thick 49 ppm $D^{35}Cl/pH_2$ solid; trace (a) is for the as-deposited sample at $T = 2.5$ K, trace (b) is during annealing at $T = 4.9$ K, trace (c) is for the sample re-cooled to $T = 2.5$ K, and (d) is for the sample warmed up to $T = 3.6$ K. The $(DCl)_n$ cluster absorptions grow irreversibly in intensity upon initial annealing, but the $P_1(1)$ and $R_1(1)$ DCl monomer features show a reversible temperature dependence.
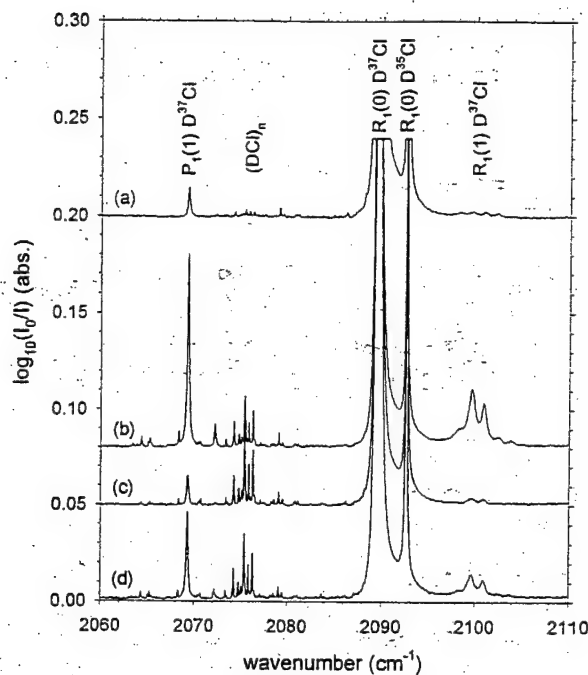
FIG. 4. Temperature dependence of $D^{37}Cl/pH_2$ monomer fundamental absorptions (0.1 cm^{-1} resolution). The sample is a 3.0-mm-thick 56 ppm $D^{37}Cl/pH_2$ solid; trace (a) is for the as-deposited sample at $T = 2.6$ K, trace (b) is during annealing at $T = 4.8$ K, trace (c) is for the sample recooled to $T = 2.6$ K, and trace (d) is for the sample warmed up to $T = 3.6$ K.
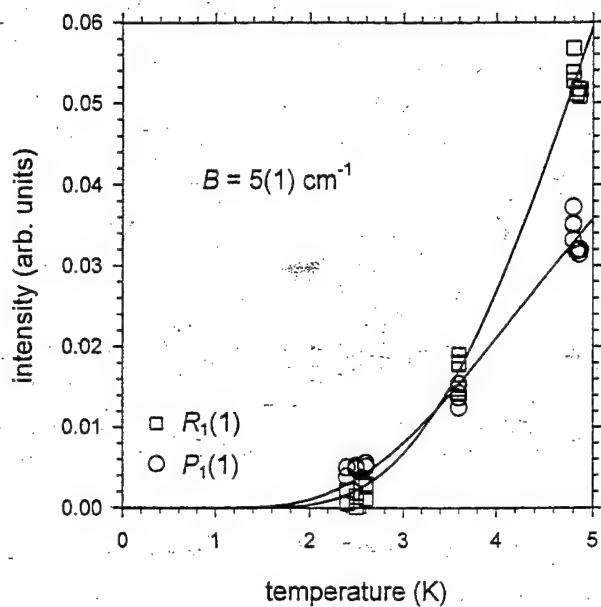
FIG. 5. Temperature dependence of the integrated intensity of the $P_1(1)$ (circles) and $R_1(1)$ (squares) DCl rovibrational transitions in DCl/pH$_2$ samples. The solid lines represent separate fits of the $P_1(1)$ and $R_1(1)$ data to Eq. 1; see the text for further details.
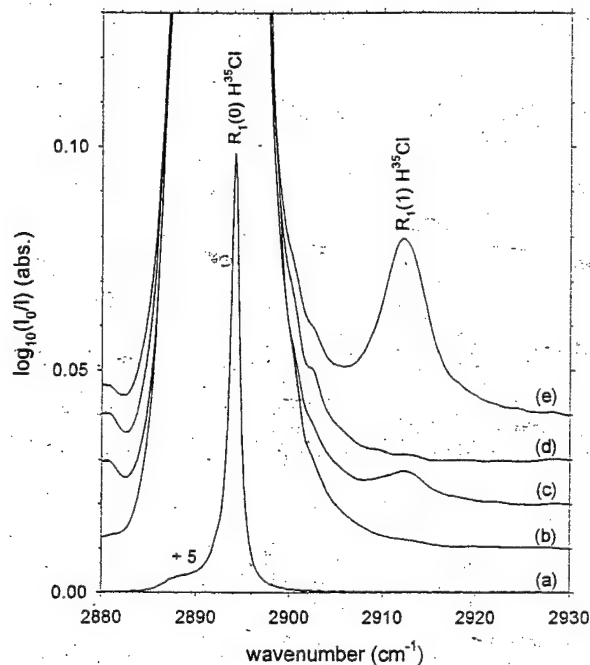
FIG. 6. $H^{35}Cl/pH_2$ monomer fundamental absorptions. Spectra for two different samples are shown (1.0 cm^{-1} resolution). Trace (a) is for an as-deposited 3.0-mm-thick 30 ppm $H^{35}Cl/pH_2$ solid at $T = 2.4$ K; the spectrum has been rescaled by a multiplicative factor of 0.2. Traces (b) through (e) are for a 3.0-mm-thick 284 ppm $H^{35}Cl/pH_2$ solid; trace (b) is for the as-deposited sample at $T = 2.4$ K, trace (c) is during annealing at $T = 4.8$ K, trace (d) is for the sample recooled to $T = 2.4$ K, and trace (e) is during the destructive sublimation of the sample at $T \approx 10$ K.
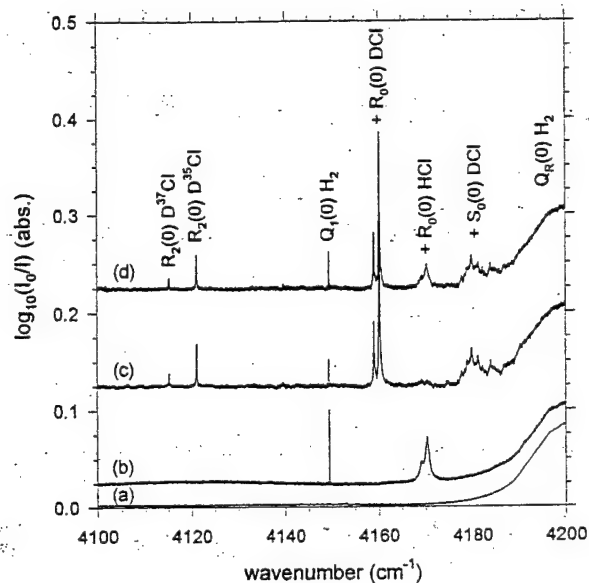
FIG. 7. Survey of HCl- and DCl-induced IR activity in solid pH_2. Trace (a) is the spectrum (0.1 cm^{-1} resolution) of a 3.1-mm-thick as-deposited 120 ppm oH_2/pH_2 solid at T = 2.4 K. The very weak feature near 4153 cm^{-1} is the $Q_1(0)$ H_2 absorption induced by residual oH_2 molecules; the broad feature at the right side of the spectrum is the rising edge of the $Q_R(0)$ H_2 phonon sideband. Trace (b) is for the as-deposited 88 ppm HCl/pH_2 sample depicted in the upper panel of Fig. 2. Trace (c) is for the as-deposited 102 ppm DCl/pH_2 sample depicted in the lower panel of Fig. 2. Trace (d) is for an as-deposited 2.9-mm-thick pH_2 sample doped with 50 ppm HCl and 100 ppm DCl at T = 2.5 K; 0.01 cm^{-1} resolution. The sharp features in traces (b) through (d) near 4149.4 cm^{-1} are the $Q_1(0)$ H_2 absorption transitions induced by the presence of HCl and DCl dopant molecules. The labels "+ $R_0(0)$ DCl," "+ $R_0(0)$ HCl" and "+ $S_0(0)$ DCl" are shorthand for the $Q_1(0)$ H_2 + $R_0(0)$ DCl, $Q_1(0)$ H_2 + $R_0(0)$ HCl, and $Q_1(0)$ H_2 + $S_0(0)$ DCl cooperative absorptions in which the dopant molecules undergo a pure rotational transition. Traces (c) and (d) also show the $R_2(0)$ DCl vibrational overtone transition.
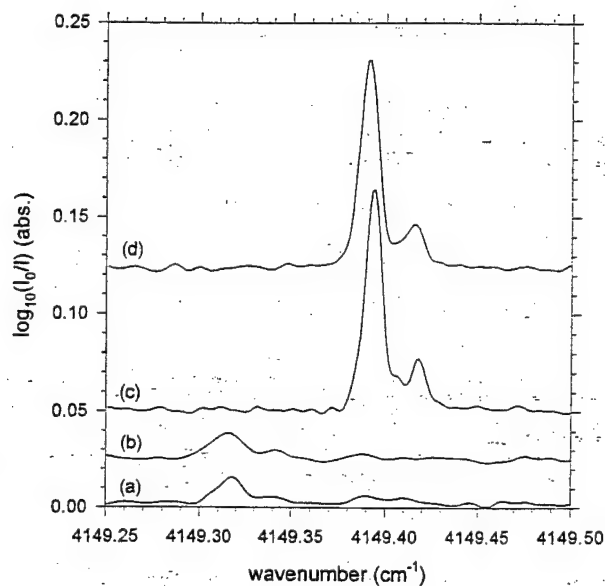
FIG. 8. Isotope dependence of the $Q_1(0)$ H_2 + $Q_0(0)$ HCl induced IR absorptions. Trace (a) is

the spectrum (0.01 cm^{-1} resolution) of an as-deposited 3.0-mm-thick 49 ppm D^{35}Cl/pH$_2$ solid at T

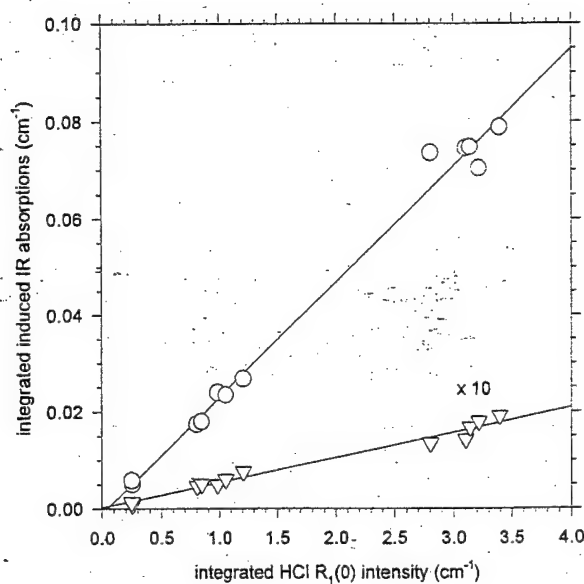= 2.5 K. Trace (b) is the spectrum (0.01 cm^{-1} resolution) of an as-deposited 3.0-mm-thick 56

ppm D^{37}Cl/pH$_2$ solid at T = 2.5 K. Trace (c) is the spectrum (0.005 cm^{-1} resolution) of an as-

deposited 3.0-mm-thick 90 ppm H^{35}Cl/pH$_2$ solid at T = 2.4 K. Trace (d) is the spectrum (0.005

cm^{-1} resolution) of an as-deposited 2.9-mm-thick 94 ppm H^{37}Cl/pH$_2$ solid at T = 2.4 K.

FIG. 9. Correlation plot of integrated intensities of direct and induced IR absorptions in dilute, as-deposited HCl/pH$_2$ solids. The circles are for the $Q_1(0)$ H$_2$ + $R_0(0)$ HCl transition near 4170 cm^{-1}, the triangles are for the sharp $Q_1(0)$ H$_2$ transition near 4149.4 cm^{-1}; the latter have been rescaled by a multiplicative factor of 10.
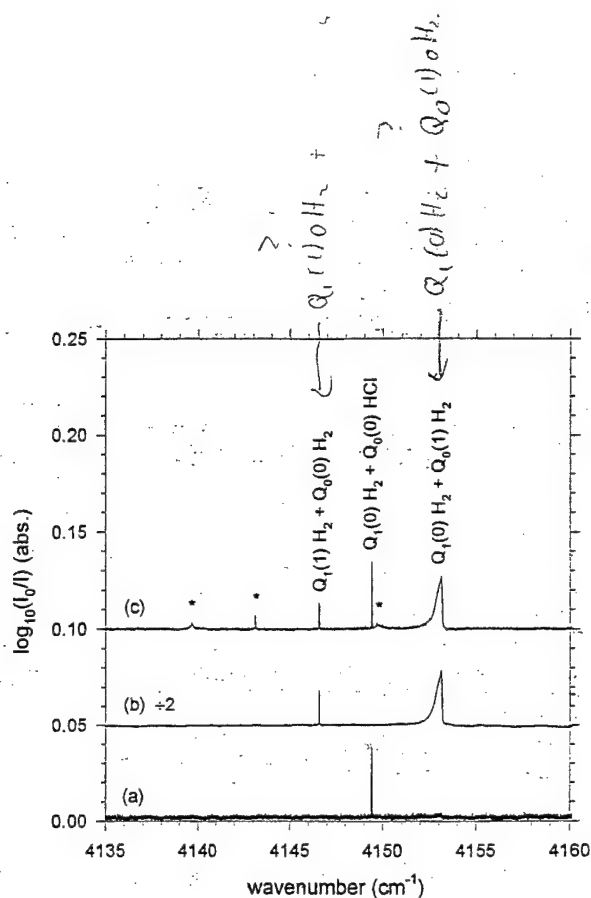
FIG. 10. oH_2 and $H^{37}Cl$ induced IR activity in solid pH_2. Trace (a) is the spectrum (0.005 cm^{-1} resolution) of an as-deposited 3.0-mm-thick 33 ppm $H^{37}Cl/pH_2$ solid at $T = 2.4$ K. Trace (b) is the spectrum (0.008 cm^{-1} resolution) of an as-deposited 4.0-mm-thick 2800 ppm oH_2/pH_2 solid at $T = 2.5$ K; this spectrum has been rescaled by a multiplicative factor of 0.5. Trace (c) is the spectrum at $T = 2.4$ K (0.01 cm^{-1} resolution) of an as-deposited 3.0-mm-thick pH_2 solid doped with 52 ppm ppm $H^{37}Cl$ and 1200 ppm oH_2. The features marked by asterisks near 4139.65, 4143.11, and 4149.66 cm^{-1} only appear in the sample doped with both HCl and oH_2.
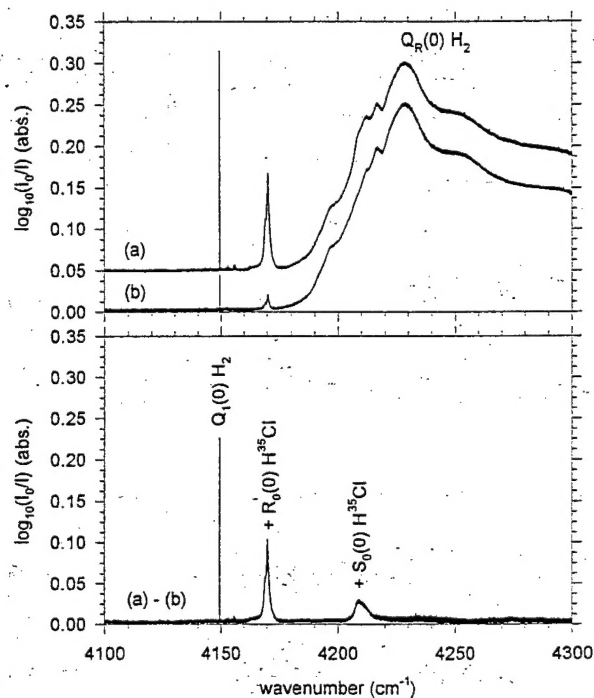
FIG. 11. $H^{35}Cl$-induced IR activity in solid pH_2 (0.005 cm^{-1} resolution). Trace (a) depicts an as-deposited 3.0-mm-thick 30 ppm $H^{35}Cl/pH_2$ solid at $T = 2.4$ K; trace (b) depicts an as-deposited 3.0-mm-thick 284 ppm $H^{35}Cl/pH_2$ solid as-deposited at $T = 2.4$ K. The lower panel shows the direct subtraction of trace (b) from trace (a). Cancellation of the broad $Q_R(0)$ phonon sideband reveals the weak $Q_1(0)$ H_2 + $S_0(0)$ HCl cooperative absorption near 4209 cm^{-1}.
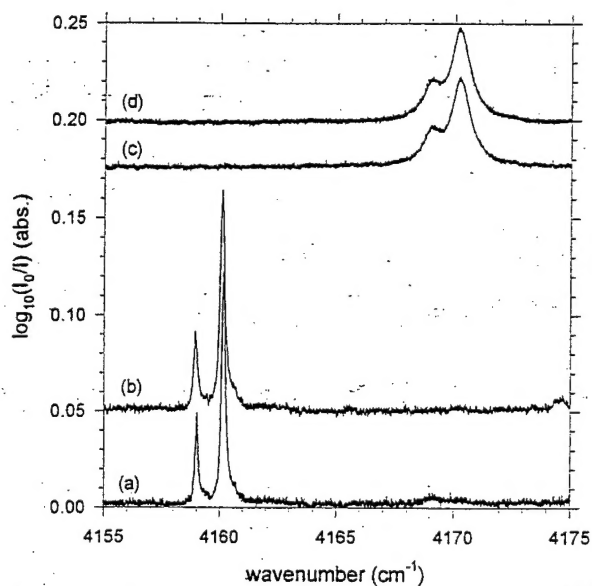
FIG. 12. Isotope dependence of the $Q_1(0)$ $H_2 + R_0(0)$ HCl (DCl) induced IR absorptions. Trace (a) is the spectrum (0.01 cm^{-1} resolution) of an as-deposited 3.0-mm-thick 49 ppm $D^{35}Cl/pH_2$ solid at $T = 2.5$ K. Trace (b) is the spectrum (0.01 cm^{-1} resolution) of an as-deposited 3.0-mm-thick 56 ppm $D^{37}Cl/pH_2$ solid at $T = 2.5$ K. Trace (c) is the spectrum (0.005 cm^{-1} resolution) of an as-deposited 3.0-mm-thick 90 ppm $H^{35}Cl/pH_2$ solid at $T = 2.4$ K. Trace (d) is the spectrum (0.005 cm^{-1} resolution) of an as-deposited 2.9-mm-thick 94 ppm $H^{37}Cl/pH_2$ solid at $T = 2.4$ K.

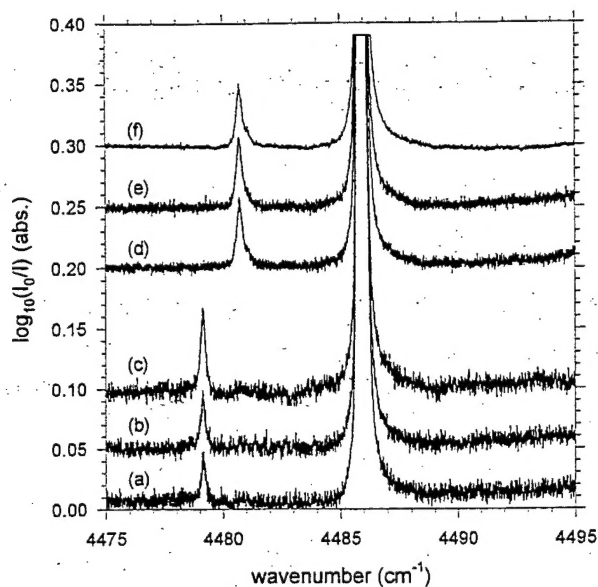FIG. 13. Isotope dependence of the $S_1(0)$ $H_2 + Q_0(0)$ HCl (DCl) induced IR absorptions. Trace (a) is for the 49 ppm $D^{35}Cl/pH_2$ sample depicted above in Fig. 12 (a). Trace (b) is for the 56 ppm $D^{37}Cl/pH_2$ sample depicted in Fig. 12 (b). Trace (c) is for the 102 ppm DCl/pH_2 sample depicted in trace (a) of the lower panel of Fig. 2. Trace (d) is for the 90 ppm $H^{35}Cl/pH_2$ sample depicted in Fig. 12 (c). Trace (e) is for the 94 ppm $H^{37}Cl/pH_2$ sample depicted in Fig. 12 (d). Trace (f) is for the 88 ppm HCl/pH_2 sample depicted in trace (a) of the upper panel of Fig. 2.
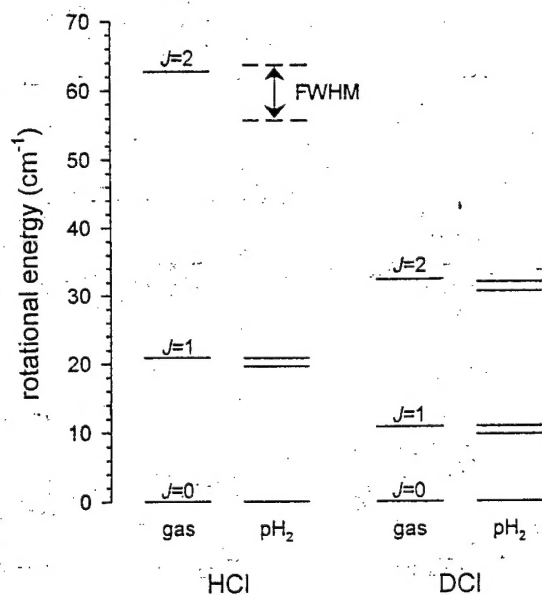
Fig. 14. Rotational energy levels of HCl and DCl in the gas phase (gas) and solvated in solid pH_2 with one vibrationally excited nearest neighbor (pH_2). Both solvated species display an approximately 1 cm^{-1} splitting of the J=1 rotational energy level. The J=2 rotational state is split into at least two resolvable sublevels for DCl, but only a broad energy range can be specified for HCl, specified by the FWHM of the observed spectral feature.